PERGAMON

International Journal of Rock Mechanics & Mining Sciences 39 (2002) 287–302

International Journal of
Rock Mechanics
and Mining Sciences

www.elsevier.com/locate/ijrmms

Experimental and numerical study of the Kaiser effect in cyclic Brazilian tests with disk rotation

A. Lavrov[a,b,*], A. Vervoort[a], M. Wevers[c], J.A.L. Napier[d]

[a] *Department of Civil Engineering, Faculty of Applied Sciences, Catholic University of Leuven, Kasteelpark Arenberg 40, B-3001 Leuven, Belgium*
[b] *Physical and Engineering Department, Moscow State Mining University, Moscow, Russia*
[c] *Department of Metallurgy and Materials Engineering, Catholic University of Leuven, Belgium*
[d] *CSIR, Miningtek, South Africa*

Accepted 18 March 2002

Abstract

Sensitivity of the Kaiser effect to the deviations of the directions of σ_1-principal stress experienced by rock in successive loading cycles has an important impact on the application of this effect for stress measurements in rocks. The paper presents an analysis of the gradual Kaiser effect degradation with increasing deviation of the principal stress axes between loading cycles in Brazilian experiments. An experimental study was carried out to investigate the Kaiser effect in cyclic loading tests of disk specimens of a brittle limestone in diametrical compression with acoustic emission measurement. Tests were performed in which disks were loaded in two cycles without or with rotations between successive cycles. The rotation angle varied between 0° and 90°. The Kaiser effect became gradually less pronounced with increasing rotation angle, but remained detectable for angles $<10^\circ$. Rotation by more than 10° resulted in complete disappearance of the effect. These experimental results were confirmed by numerical simulations using the displacement discontinuity method.

Keywords: Kaiser effect; Fracture; Limestone; Principal stress direction; Experiment; Numerical simulation; Brazilian test

1. Introduction

From a practical point of view, the Kaiser effect is one of the most important and interesting manifestations of the fundamental ability of rocks and materials to accumulate, to retain and to reproduce information on the peak stresses and strains experienced in the past [1–3]. This ability called 'stress memory' or 'end-point-memory' has attracted attention as a possible basis for stress measurement in rocks [4–6]. Moreover, stress memory is considered to be one of the most characteristic features of natural heterogeneous materials indicating their non-classical non-linear behaviour [7–9].

In its simplest form, the Kaiser effect can be observed in rocks and materials during their cyclic uniaxial loading by acoustic emission (AE) measurements. As soon as the load achieves its previously reached peak value, a noticeable increase in AE activity takes place and the AE hit rate (number of AE signals per time unit) increases dramatically. This leads to an inflexion (change of slope) in the cumulative hits vs. stress curve. The quality of the Kaiser effect under cyclic uniaxial conditions is usually quite high over a wide range of stresses from about 30% to about 80% of the strength. It is expressed by the Felicity ratio (*FR*), which is the ratio of the stress value corresponding to the inflexion point in the AE cumulative hits vs. stress curve, to the previous peak stress (Fig. 1a). The *FR* can also be defined as the ratio of the stress value at which a steadily increasing AE activity begins, to the previous peak stress (Fig. 1b) [10]. In this study, both ways of the *FR* computation were implemented, depending on whether the cumulative hits vs. load curve could be well approximated by two straight lines, or whether an onset of steadily increasing AE could be well identified. In the case of a perfect Kaiser effect, *FR* equals unity. Felicity ratio less than unity indicates a distortion of the Kaiser effect.

*Corresponding author. Department of Civil Engineering, Faculty of Applied Sciences, Catholic University of Leuven, Kasteelpark Arenberg 40, B-3001 Leuven, Belgium. Tel.: +32-16-32-1665; fax: +32-16-32-1988.

E-mail address: alexander.lavrov@bwk.kuleuven.ac.be (A. Lavrov).

1365-1609/02/$ - see front matter
PII: S1365-1609(02)00038-2

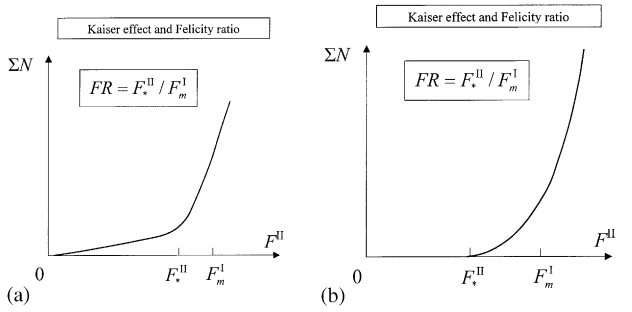

Fig. 1. Definitions of Felicity ratio: (a) when the cumulative hits vs. load curve can be approximated by two straight lines; (b) when a steadily increasing AE activity begins at a certain load level F_*^{II}: σN—cumulative AE hits in the second cycle; F^{II}—second-cycle load; F_m^I—maximum load of the first cycle; F_*^{II}—load value at which the Kaiser effect takes place in the second cycle (onset of steadily increasing AE activity).

When applying the Kaiser effect for the determination of geo-stresses, rock specimens are taken from in situ and tested in the laboratory, usually in uniaxial conditions. AE is continuously measured during the test. Then, the cumulative AE hits vs. stress curve is interpreted in the hope of finding a characteristic inflexion indicating that the test stress has reached the actual in situ stress level. This simple procedure was employed with some success in the 1970s. However, the important role of the triaxial stress state in the formation of stress memory and of the Kaiser effect was eventually recognized [2,11–13]. Since then, comprehensive experimental [2,4,13–15] and theoretical [11,16–21] studies were carried out in order to investigate the stress memory and damage surface formation under triaxial stress conditions.

It should be noted that all of the above-mentioned studies concentrated on the investigation of the Kaiser effect when principal stress directions are the same in successive loading cycles. However, it is important to know the Kaiser effect features in case of deviation, or rotation of principal stress axes in the successive loadings as well. The relevance of this question is due to the fact that usually one does not know exactly the direction of the principal stress axes before making stress measurement tests, except in special cases (e.g. horizontal deposits of bedded rocks). In some cases, the direction of the maximum compressive principal stress may be incorrectly estimated beforehand. In some situations, the direction of σ_1 cannot be evaluated a priori even approximately (e.g. in the areas with increased tectonic activity, domes and around underground openings). This makes it important to know how sensitive the Kaiser effect is to the deviation of the principal stress directions in the second cycle from the principal axes in the first one.

Only a few attempts to clarify this question are known to the authors [22–24]. In these works, the Kaiser effect was studied on cubic rock specimens which were consecutively loaded along perpendicular directions. In each cycle, the specimen was uniaxially loaded on one side of the cube, then completely unloaded, and another uniaxial load cycle was performed on another side of the cube. No Kaiser effect was observed in the second cycle. It was thus concluded that damage (and stress memory) created in uniaxial compression in one of the directions cannot be revealed by uniaxial reloading in a perpendicular direction. This conclusion seems to be in good agreement with the ideas about anisotropic damage formation in brittle rocks [11,16,17]. Intermediate directions (between 0° and 90°) have not been experimentally studied so far. Theoretical predictions say, however, that the Kaiser effect should be quite sensitive to even very small rotations of the principal stress axes and should practically disappear when the rotation angle of the σ_1-axis is more than 10–20° [11,16]. This important theoretical conclusion needed a direct experimental verification, which is the main subject of this paper.

The experimental verification of the directional dependency of the Kaiser effect is accomplished by testing disk specimens of a brittle rock (crinoïdal limestone) in diametrical compression (Brazilian mode), with or without disk rotation between two loading cycles. By using diametrically stressed disk specimens instead of uniaxial tests on, e.g. prismatic or cubic specimens (with additional cutting at different angles between cycles) additional damage is avoided which could be introduced in the rock during cutting. It should certainly be kept in mind that the Brazilian loading mode is different from uniaxial or triaxial compression. However, the results from Kaiser effect studies of principal stress rotation obtained in Brazilian tests could create a basis for conclusions about rotation effects in pure compressive stress conditions.

To clarify what is being observed in the experiments, numerical simulations are performed using the displacement discontinuity (DD) method. The DD method being a boundary-element method enables one to simulate fracture initiation and growth in brittle materials subjected to loading with prescribed boundary conditions. Explicit account for crack interaction and strength inhomogeneity of rock makes this method a powerful tool in the simulation of rock fracture phenomena and fracture paths during various loading regimes, both monotonic and cyclic [25,26]. The discontinuity interaction and growth simulation (DIGS) code developed originally to simulate mining induced fracturing [26] is applied for the simulation of the Kaiser effect in Brazilian disks subjected to two loading cycles with or without disk rotation.

It should be noted that this work is not aiming at an immediate practical application of the Kaiser effect in general and of the results obtained in particular. The revealed high sensitivity of the Kaiser effect to the

rotations of principal stresses creates some difficulties in the practical application of the effect for stress measurements as it is usually performed at present.

The paper is structured in the following way. First, experimental equipment and procedure are described (Section 2). Then results of the tests are presented (Section 3), followed by the DIGS simulations of the Kaiser effect in diametrically loaded disks without and with rotation between cycles (Sections 4 and 5, respectively). The paper is completed by a discussion and conclusions in Sections 6 and 7.

2. Experimental set-up and equipment

The tests were performed on specimens of the Belgian 'blue' limestone also called 'petit granit'. This is a practically monomineralic crinoïdal limestone (>95% calcite) having very low porosity (<0.5%). The rock is composed of crinoïds (ca. 80%) and micrite, the latter building a fine-crystalline matrix in which the crinoïds are placed. Traces of quartz, dolomite and iron sulphides are also present. The rock is a typical brittle solid having a uniaxial compression strength of 100–130 MPa and a tensile strength of about 15 MPa.

One of the problems in the Kaiser effect studies is that a rock may contain memory on the stresses experienced in situ. The specimens in this study were taken from a quarry near the Earth's surface. Hence, the recent stresses in this rock are negligible or, at least, by far smaller than the stresses applied during laboratory testing program. Stresses that were acting during geological history cannot be neglected, but stress memory and the Kaiser effect are known to disappear in the course of time. Separate experiments have shown that the time-dependent decay of the Kaiser effect in this type of limestone occurs quite quickly: stress memory disappears after a-few-month rest [41]. This allowed us to consider the specimens as being 'fresh' to provide the necessary purity of the tests.

Disk specimens having a diameter of 113 mm and a thickness of approximately 20 mm were cut from a block such that their planes were parallel to the bedding. It should be noted that the diameter-to-thickness ratio of 5.65 used in this work does not agree with ISRM recommendations given, e.g. in Ref. [27], according to which it must be equal to 1.0. However, for research purposes, it was better to use high diameter-to-thickness ratio specimens in order to make the state of the disk closer to plane stress rather than plane strain. This makes the stress distribution along the thickness of the disk more homogeneous. Similar thin specimens were used, e.g. in Refs. [28,29]. In order to make the zone, in which tensile stresses act, wider, hardboard inserts were placed between the disk and the platens of the loading machine. This resulted in a contact angle of 20–25°.

The loading of disk specimens was carried out using a displacement-controlled testing machine of type INSTRON 1196 which could provide a compressive load of up to 250 kN. AE was continuously measured throughout the tests using an AMS3 system by Vallen-Systeme GmbH. Two wide-band AE sensors of type B1025 (Digital Wave Corp., USA) having a frequency range from 50 kHz to 2 MHz were attached to the specimen symmetrically with respect to the main diameter of the disk, as shown in Fig. 2. This allowed a 'linear' location of AE sources to be performed in the sense that it is possible to distinguish between AE sources situated in the central zone of the specimen (along the main diameter) and those coming from the peripheral parts. For the sake of attachment convenience, AE sensors were placed not on the very edge of the disk but a bit towards the centre as shown schematically in Fig. 2. The distance between the sensors usually ranged between 7 and 8 cm in the tests.

The velocity of longitudinal elastic waves used for the location calculations was 5450 m/s. Anisotropy of the velocity was studied on several specimens prior to the tests, and it was found that the velocity anisotropy does not exceed 5% in this rock. Low anisotropy is one of the prerequisites for the location reliability.

Being received and converted into electric pulses, AE signals ('hits') were amplified by pre-amplifiers with a gain of 40 dB. The threshold level of 40.5 dB was used to get rid of the environmental noise and of the signals coming from the testing machine (if any). The correctness of the chosen threshold was proved by the presence of a clear Kaiser effect in the tests without rotation as described further. The threshold measured in dB had to be referred to the 1 μV pre-amplifier input.

An analog-to-digital converter incorporated in the AMS3 system had a sampling rate of 5 MHz and a

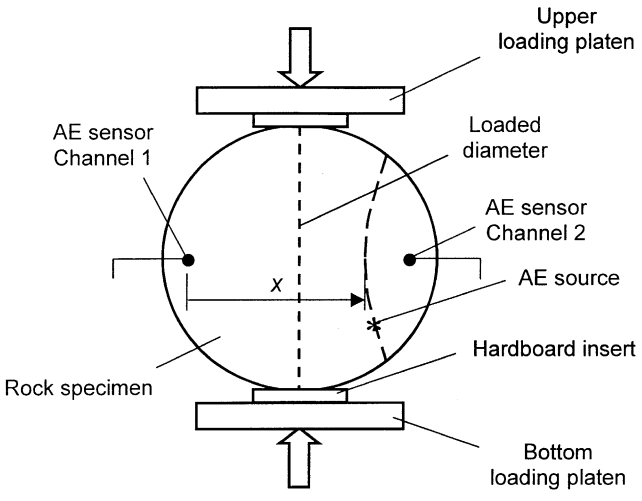

Fig. 2. Disk specimen loaded in diametrical compression. *X*-coordinate is specified as the horizontal distance from AE sensor (channel 1) to the hyperbola on which AE source is located.

dynamic range of 78 dB. A built-in band-pass filter had a frequency range from 200 to 1000 kHz. Signal parameters (duration, amplitude) were determined during on-line data processing and stored in a primary data file. The following off-line data processing was carried out using Visual AE Vallen Software (Release R2000).

A standard procedure of AE non-destructive tests was employed to eliminate signals caused by electromagnetic noise as well as signals coming from an imperfect attachment of AE sensors. This was done by analysing hit duration vs. hit amplitude distributions like described, for example, in Ref. [29]. It should be noted that in most tests there was only one correlation cloud with a correlation coefficient of 0.8–0.9, indicating no electromagnetic interferences and no or very little noise coming from the attachment of the sensors. Once a second (much smaller) cloud or outstanding events were present, they were removed from the following off-line analysis.

For the Kaiser effect identification, dependencies of the cumulative hits vs. load were plotted based on the acquired data. It was found that these dependencies are more reliable indicators of the Kaiser effect than energy vs. load or hit rate vs. load. Big single events induced, e.g. by spalling in contact zones can affect the cumulative energy a lot. These jumps in the energy can be misinterpreted as a Kaiser effect. On the other hand, they do not contribute to the cumulative hits so much.

The use of the cumulative hits was preferred above the hit rate as the latter usually contains irregular fluctuations (noise) which are smoothed by integrating.

The Kaiser effect was studied during two-cycle tests on disk specimens. The aim of the tests was the investigation of the influence of the rotation between two cycles on the Kaiser effect in the second cycle. Rotation angles of 0° (i.e. without rotation), 3.5°, 7.5°, 15°, 30°, 45°, 60° and 90° were studied. Two to four specimens were tested for each of these angles. The consistency of the results for each angle was quite good, so a bigger number of tests per angle seemed to be unnecessary. The first cycle was carried out to a peak load corresponding to 50–70% of the strength in the Brazilian testing mode. It was established that, like many other rocks, the limestone exhibits the best-pronounced Kaiser effect in this load range ($FR \approx 1.0$). The second cycle was conducted till failure. In case of rotation angles $<30°$, AE sensors were not reinstalled between the cycles. This allowed us to keep the coupling conditions 'sensor–rock' the same in the first and second cycle. Normally, when the sensors are reinstalled in a new position, the coupling conditions can change which makes it impossible to draw a comparison between absolute values of the AE activity in different loading cycles. This is because reinstalling the sensors leads to a change in the force with which the sensors are pressed to the rock (unless some special accessories are used, like calibrated springs). Moreover, the thickness of the grease layer which is put between sensor and rock may be different. The mineral grains on which the sensors stand in the new position are different, too, from those in the old position, which implies a difference in the acoustic impedance and, hence, in the reflexion coefficient. Altogether, it means that, by the same threshold level used throughout the tests, some of the AE pulses which would surpass in one of the loading cycles, might be rejected in another one due to a different (worse) coupling, and vice versa. Therefore, it was sensible to compare absolute values of the AE activity (hit rate) in successive loading cycles only in the tests, in which the AE sensors were not reinstalled, i.e. for rotation angle smaller than 30°.

3. Experimental results

First of all, cyclic loading tests without disk rotation between cycles were carried out. Zero rotation between cycles resulted in a very well-pronounced Kaiser effect (Fig. 3). In the test shown in Fig. 3, the load was raised in the first cycle from zero to a peak value of 40 kN, which was about 80% of the ultimate strength. AE

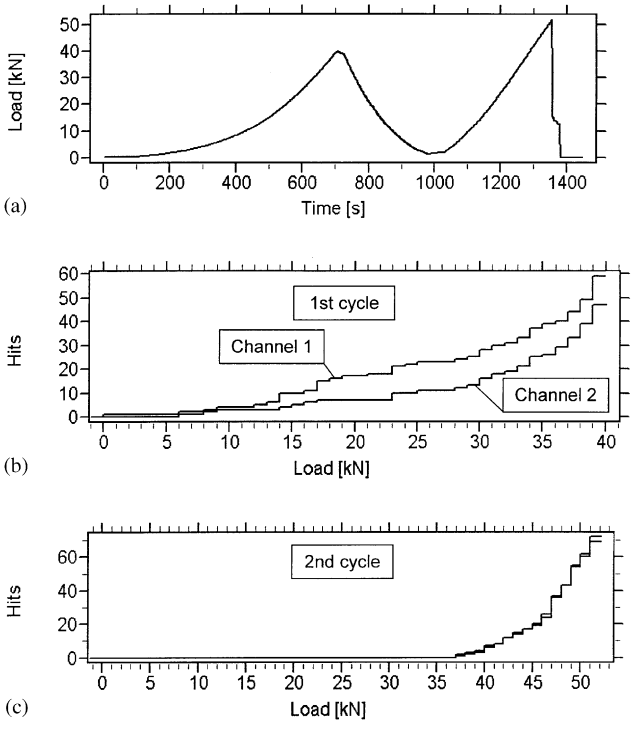

Fig. 3. Load vs. time (a), cumulative AE hits vs. load in the first (b) and second (c) loading cycles of a disk specimen. No rotation between first and second cycle. Peak load in the first cycle is 40 kN. Ultimate load in the second cycle is 51.8 kN. Kaiser effect in the second cycle is at 37 kN; $FR = 0.925$; disk thickness 20.5 mm, diameter 113 mm and displacement rate 0.2 mm/min in both cycles.

pulses appeared first at about 5–10 kN in the first cycle (Fig. 3b). Reloading in the second cycle in the same direction as in the first one resulted in zero AE, while the load was less than 37 kN. Steadily increasing AE appeared in the second cycle as soon as this load value was surpassed (Fig. 3c). Hence, the Kaiser effect took place with a Felicity ratio of $FR = 0.925$. For rock materials, this value of the Felicity ratio indicates a quite good quality of the Kaiser effect.

Rotation by 3.5° resulted in a different manifestation of the Kaiser effect (Fig. 4), but certainly not in a total elimination. In the second cycle, the AE activity starts virtually from the beginning of loading, like in the first cycle. At the load value corresponding to the first-cycle peak value (27 kN), an inflexion (change in slope) in the cumulative hits vs. load is seen in the second cycle (Fig. 4c). This is the Kaiser inflexion. The inflexion is unambiguously recognized in Fig. 4c, in spite of the masking AE activity at lower load values. The AE cumulative curve in Fig. 4c can be interpolated by two straight lines whose intersection approximately indicates the peak load of the first cycle. The Felicity ratio can be determined here as a ratio of the load at which the two straight lines intersect in the second cycle, to the peak load of the first cycle (see Fig. 1a). Defined in this way, the Felicity ratio is close to unity in Fig. 4c.

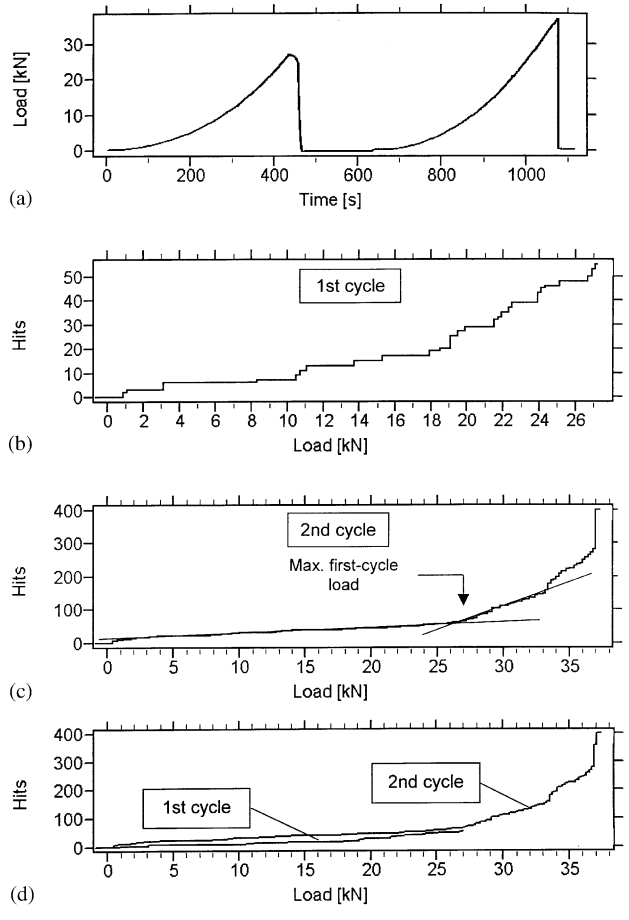

Fig. 4. Load vs. time (a), cumulative AE hits vs. load in the first (b), second (c) and both (d) loading cycles of a disk specimen. Rotation by 3.5° between first and second cycles. Peak load in the first cycle is 27 kN. Ultimate load in the second cycle is 37.1 kN. Kaiser effect in the second cycle is at 27 kN; $FR = 1.0$; disk thickness 18.5 mm; diameter 113 mm and displacement rate 0.2 mm/min in both cycles.

The fact that the AE sensors were not reinstalled after the 3.5° rotations allows an absolute comparison between AE activity in the first and second cycle. This is shown in Fig. 4d. It is clear that the AE activity in the second cycle at load levels less than or equal to the peak first-cycle load is greater than the activity observed in the first cycle. This higher second-cycle AE activity should be attributed to the natural inhomogeneity of rock.

Rotation by 7.5° resulted in a further distortion of the Kaiser effect. The noise at lower load values in the second cycle increases. However, it is still possible to identify the effect (see smooth inflexion in Fig. 5a and the onset of steadily increasing AE activity in Fig. 5b). The Felicity ratio is about unity in both figures, although the identification of the inflexions is more complicated in comparison to the cases where the rotation was zero and 3.5°.

Increasing the rotation angle to 15° resulted in a total disappearance of the Kaiser effect. This is clearly seen in Fig. 6. Cumulative AE vs. load curves do not indicate any inflexions or other characteristic points during the entire loading in the second cycle. Similar results were obtained when the disks were rotated by 30°, 45°, 60° or 90° between cycles. The second-cycle AE signatures for those specimens looked the same as would arise from

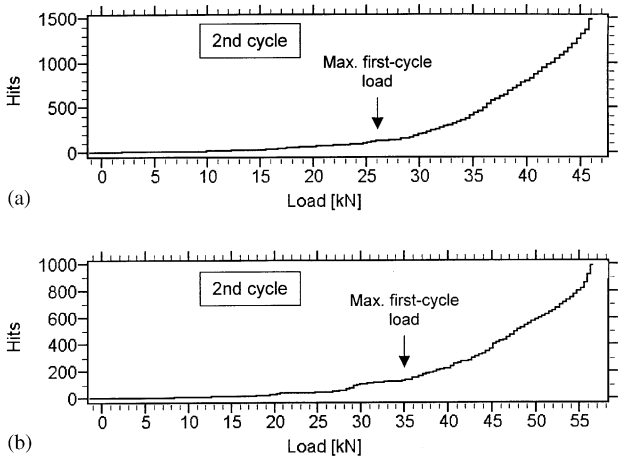

Fig. 5. Cumulative AE hits vs. load in the second cycle in two tests. Rotation by 7.5° between first and second cycles in both tests. Displacement rate 0.2 mm/min in all tests. (a) Peak load in the first cycle is 26 kN. Ultimate load in the second cycle is 46.2 kN. Kaiser effect in the second cycle is at 28 kN; $FR = 1.08$; disk thickness 19.3 mm; diameter 113 mm. (b) Peak load in the first cycle is 35 kN. Ultimate load in the second cycle is 56.5 kN. Kaiser effect in the second cycle is at 35 kN; $FR = 1.0$; disk thickness 22.0 mm; diameter 113 mm.

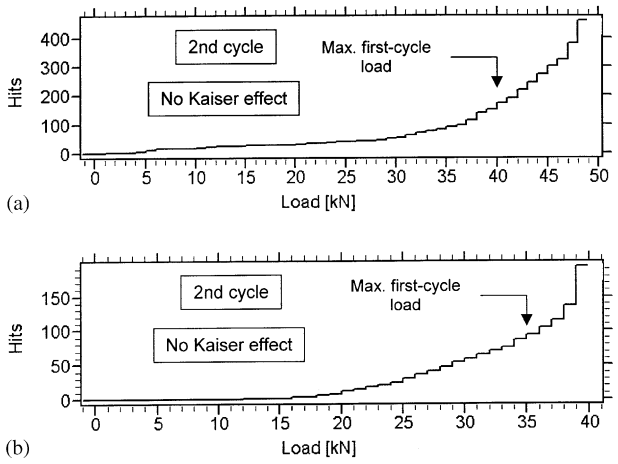

Fig. 6. Cumulative AE hits vs. load in the second cycle in two tests. Rotation by 15° between first and second cycles in both tests. Displacement rate 0.2 mm/min in all cycles. (a) Peak load in the first cycle is 40 kN. Ultimate load in the second cycle is 48 kN. No Kaiser effect in the second cycle. Disk thickness 20.0 mm; diameter 113 mm. (b) Peak load in the first cycle 35 kN. Ultimate load in the second cycle 39.6 kN. No Kaiser effect in the second cycle. Disk thickness 19.1 mm, diameter 113 mm.

'fresh' specimens, without the first-cycle pre-loading, i.e. AE was smoothly increasing with increasing load in the second cycle and no inflexions or any other anomalies were observed in the AE behaviour.

In conclusion, the experiments have demonstrated a high sensitivity of the Kaiser effect to the rotation of the principal loading directions in disk specimens. The Kaiser effect becomes less clear when the rotation angle increases from 0° to 7.5°, but it is still detectable over this range of angles. Increasing the rotation angle to 15° or more results in the entire disappearance of the Kaiser effect.

4. DIGS simulations of microfracturing processes and AE activity in cyclically loaded Brazilian disks without rotation

Numerical simulations described in this section were performed using a two-dimensional boundary element code DIGS that makes use of the displacement discontinuity method. Principles and features of the DD method are described in [30] and features of the DIGS simulation code are described in detail in Refs. [25,26,31] and therefore are only briefly discussed here. In Ref. [31], the code was successfully used to simulate fracture paths and stress–strain behaviour of brittle rocks subjected to confined tests. In Refs. [32,33], a monotonic loading of disk specimens to ultimate failure was simulated by DIGS. Realistic data regarding fracture paths were obtained.

The basic ideas of the DIGS code are as follows. The medium under simulation is assumed to be a linear elastic solid. All non-linearity is introduced by DDs, which can be considered to represent microcracks in real rock. The DDs are introduced only in certain places, namely along the elements of a tessellation mesh. The tessellation mesh can be defined arbitrarily but in this paper is generated as a Voronoi cell structure with an internal triangulation [31]. The mesh is generated before the simulation is started. The elements of the mesh thus indicate potential sites for the formation of cracks in the medium. During the course of a simulation exercise, loads are applied incrementally in successive loading steps to the model boundaries and crack movements are computed at all activated sites that have been selected from the tessellation mesh. For each loading step, several crack growth steps are considered. In each crack growth step, stresses are computed at designated points (termed collocation points) within each mesh element that is not yet activated. These stress values are then used to determine whether the element should be activated according to a specified strength criterion and a pre-defined priority rule [31,33]. The Coulomb–Mohr criterion is used in this paper. Elements are analysed to determine the one with the most critical stress conditions. This element loses cohesion, and the equilibrating slip or crack opening displacement discontinuity value is computed. This crack growth cycle is repeated until there are no more elements to be activated at the applied boundary conditions (i.e. at the given loading step). Then the boundary condition is changed (e.g. the displacement of the loading platen is further increased) and the process is repeated.

The DIGS simulations described here focus on the cyclic loading of disk specimens. First of all, cyclic loading of a disk without rotation between cycles was simulated. A disk of 50 mm diameter was 'loaded' between two inserts, each having a thickness of 5 mm. The inserts were placed between the disk specimen and the loading platens. Rock heterogeneity with respect to strength parameters was modeled by tessellating the entire disk using 6783 elements, of which 679 (10%) were assigned reduced strength properties ('flaws'). Three types of elements were introduced: side elements of the polygons (cohesion 70 MPa, angle of internal friction 35°, tensile strength 25 MPa), internal elements placed inside the polygons (cohesion 110 MPa, angle of internal friction 35°, tensile strength 25 MPa) and 'flaws' (cohesion 5 MPa, angle of internal friction 20°, tensile strength 5 MPa). This choice of the strength parameters yielded a tensile strength in the simulated Brazilian test of approximately 4.5 MPa. Loading was performed with controlled displacement of the upper platen, i.e. with controlled displacement of the top edge of the top insert. The bottom platen was fixed. The loading protocol in terms of displacement for a test without rotation is

shown in Fig. 7a. The displacement was increased and decreased in equal steps, namely 0.02 mm. Peak values of the displacement were 0.04, 0.08, 0.12 and 0.16 mm in the first, second, third and fourth cycle, respectively. The induced fractures (activated elements) corresponding to the peak displacements of the four cycles are shown in Fig. 8a–d, respectively. In the fourth cycle, a main crack propagates throughout the specimen.

The main fracture in Fig. 8d runs between both contact areas. It does not coincide perfectly with the main diameter and consists of parts with different orientations. At certain locations, the main fracture makes an angle of up to 90° with respect to the main diameter. This is observed also in reality, where sharp turns in the main and secondary fractures are clearly seen (Fig. 9). In the limestone specimens, such 'kinks' are due to the presence of pronounced cleavage planes in calcite grains. En passant crack interaction structures

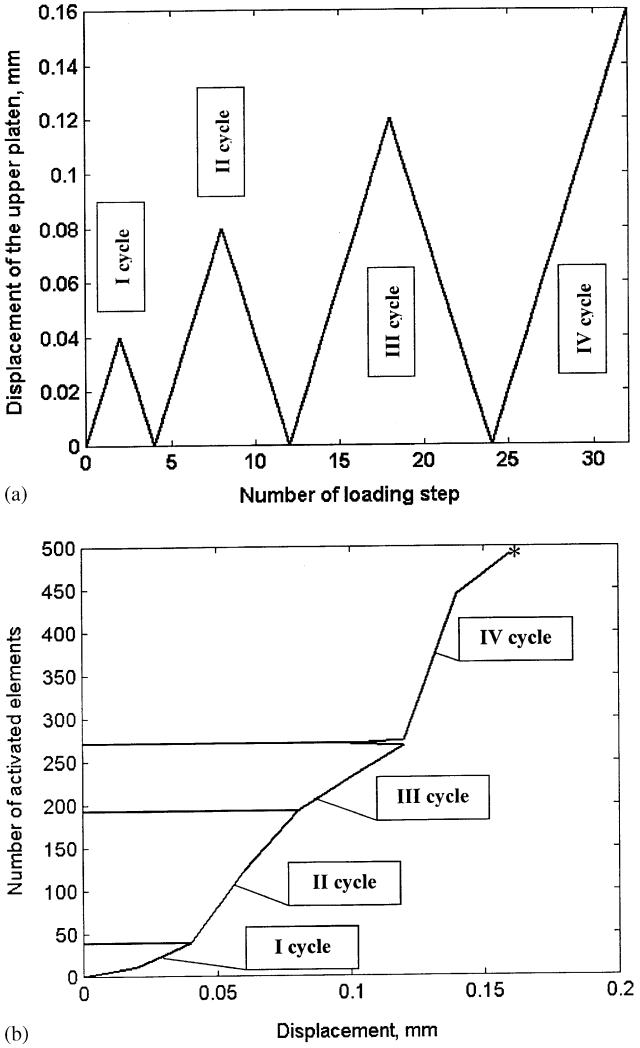

Fig. 7. Loading protocol (a) and number of activated elements vs. displacement (b) for a disk specimen cyclically loaded in diametrical compression (DIGS simulation). Displacement step 0.02 mm.

seen in Fig. 8d in the vicinity of the main fracture correspond also well with microscopic observations (Fig. 10). The joining of several cracks as it is present in the simulation results (Fig. 8) was observed also in reality near the disk–platen contact (Fig. 11). Secondary cracks running subparallel to the main diameter are clearly seen in Fig. 8d, as they were described, e.g. in Ref. [34] and observed in the tests presented here as well. Thus, the comparison of the results of DIGS simulations with microscopic observations shows a good qualitative agreement of the fracture paths observed and simulated, as was also concluded in Ref. [33].

To simulate the acoustic emission behaviour, some rules about the representation of the AE activity (cumulative number of hits) should be put forward. The simplest way to simulate AE kinetic activity consists in counting the number of elements activated at each displacement (loading) step. In this way, only breaking bonds are counted; no crack healing is simulated in the model; an element which was broken cannot break again. A similar approach was successfully implemented in, e.g. [35,36] and was employed also in the simulations described here. Some more elaborate procedures can be used to compute the released seismic energy and related parameters in rock fracture simulations [35,37,38]. In the tests of this paper, for the reasons explained in Section 2, energy was not the best suited parameter for the Kaiser effect studies. Hence, curves showing the 'number of activated elements vs. displacement' were plotted for the representation of the simulation data, the total number of activated elements representing the cumulative AE measured in the tests. An example of the simulation results for the above-described test without rotation is shown in Fig. 7b.

Cracks appear first in the vicinity of the disk–insert contact in the first cycle (Fig. 8a). This is in full agreement with the results of the earlier experiments by Falls et al. [28,39], where planar location of AE sources was performed. However, at the end of the second cycle, with the load at 50% of the strength, the AE sources are distributed over a wide range of distances from the loaded diameter (Fig. 8b), as was observed in the tests [40] (planar location in Ref. [40] allowed a distinction to be made between pulses generated at different distances from the main diameter of the disk). At the end of the third cycle, the sources are activated all over the disk except for the very periphery (Fig. 8c), again as observed in the tests [33,40]. Certainly, the density of AE sources is the highest in the central part of the specimen.

Very clear inflexions are seen in Fig. 7b in the second and third cycles indicating the Kaiser effect on the peak displacement value attained in the previous cycle. No cracks grow in the second and third cycles until the peak displacement value of the previous cycle is exceeded (peak displacement of the first or second cycle,

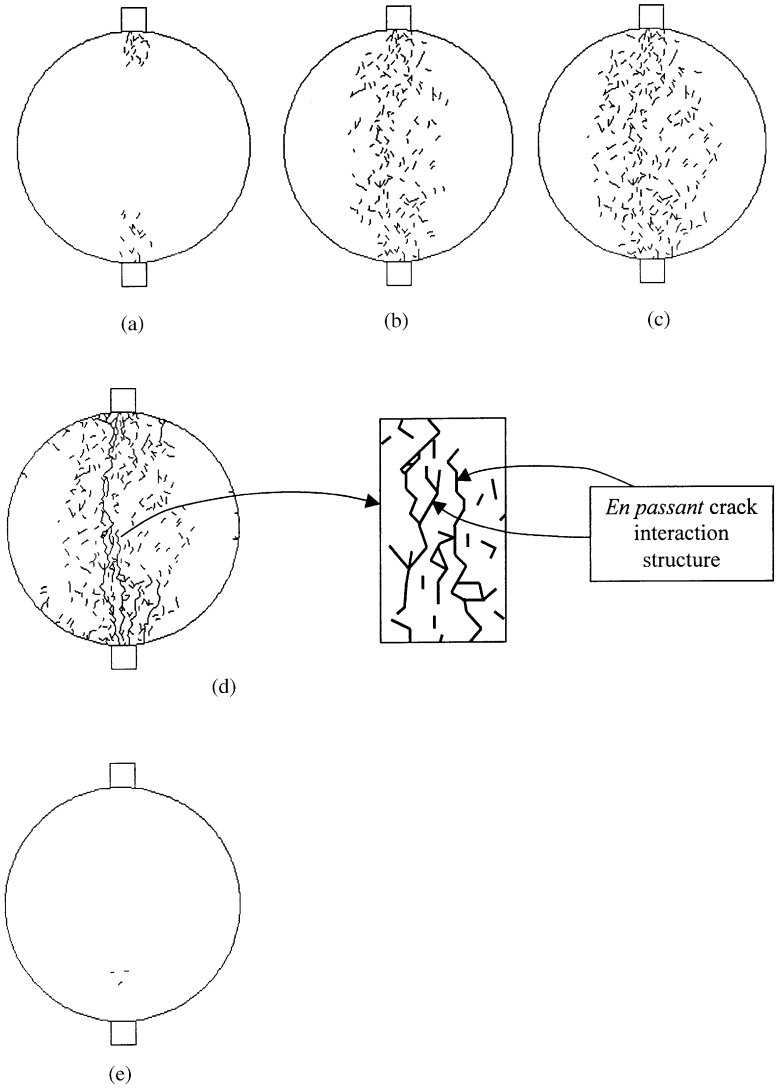

Fig. 8. Induced fractures in the simulation run shown in Fig. 7: (a)–(d)—induced fractures at the peak displacements of the first, second, third and fourth cycles, respectively (all elements activated from the beginning of the simulation to the peak of the corresponding cycle are shown); (e) elements activated during unloading from the third cycle.

respectively). In the fourth cycle, the AE pattern is slightly different, namely, some elements are activated before the peak displacement of the third cycle is surpassed (earlier onset of cracking). This is due to the crack growth observed during unloading in the third cycle. The crack growth during unloading is illustrated in Fig. 8e, where only elements activated during unloading from the peak point of the third cycle are shown. It is worthwhile to note that two of the three unloading cracks shown in Fig. 8e are orientated perpendicular to the maximum compressive stress applied during the preceding loading.

Crack growth during unloading seems to play a crucial role in making the Kaiser effect less well-pronounced (Felicity ratio <1.0). Microcracks induced during unloading cause a stress redistribution in the damaged material, which leads to an earlier onset of microcracking and AE in the following loading cycle. However, the earlier onset of cracking does not inhibit a reliable identification of the Kaiser effect in the fourth cycle in Fig. 7b. The specimen failed in the fourth cycle at the point which is shown by an asterisk in Fig. 7b.

5. DIGS simulation of microfracturing processes and AE activity in the tests with rotation

While modeling rotation tests, the same tessellation and distribution of strength properties of the elements was used as in the above-described cyclic loading without rotation.

The simulation was set up in the following way. A disk specimen was loaded to a predefined displacement value (0.08 or 0.12 mm). Then the specimen was

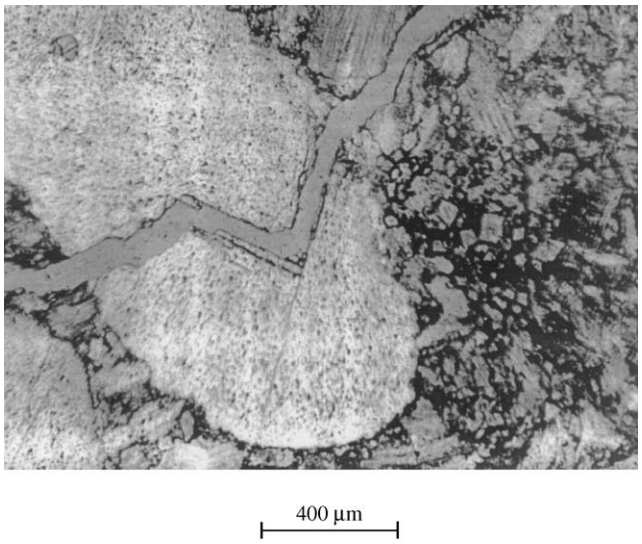

Fig. 9. Secondary fracture running along cleavage planes of a calcite crystal ('kink' structure). The dimensions of the photo are 1.2 mm × 1.8 mm. The direction of the loaded diameter of the disk is horizontal.

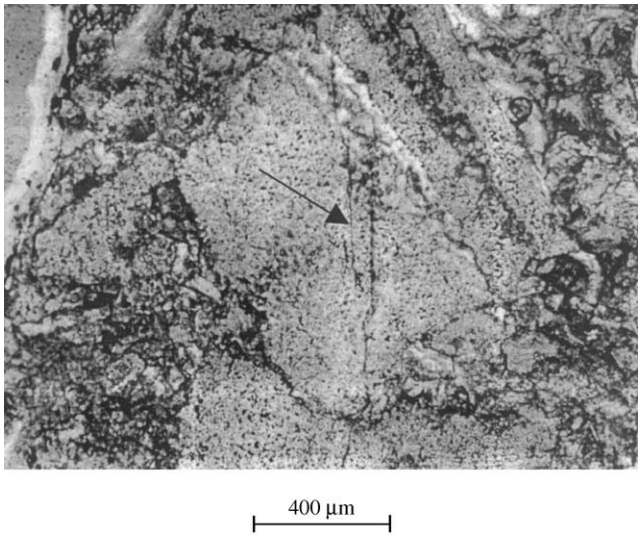

Fig. 10. En passant crack interaction structure (shown by an arrow). The dimensions of the photo are 1.2 mm × 1.8 mm. The direction of the loaded diameter of the disk is vertical.

unloaded. The inserts were re-installed in a new position corresponding to the rotation angle of θ. Then the specimen was reloaded in this new direction, until it failed. The simulations were performed for rotation angles $\theta = 4^\circ$, 8°, 16°, 30°, 46°, 60° and 90°.

In case of a 4° rotation, the Kaiser effect is present in the second cycle, but its manifestation is not so pronounced as without rotation (Fig. 12). This is valid for both first-cycle displacement values (0.08 mm in Fig. 12a and 0.12 mm in Fig. 12b). This less-pronounced Kaiser effect is seen in the form of an earlier onset of AE

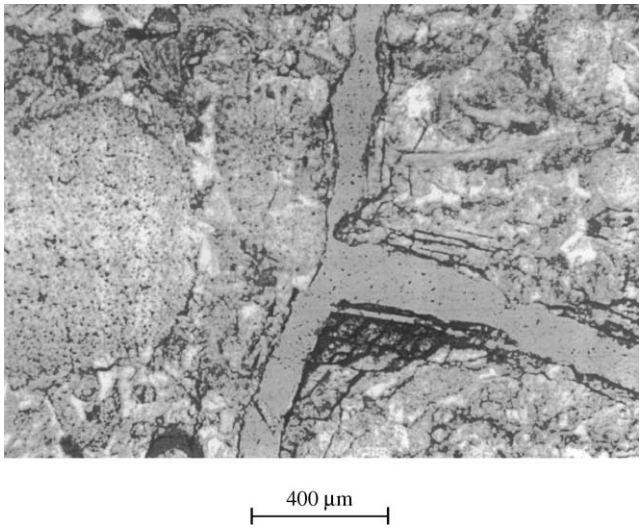

Fig. 11. Joining of several macrocracks. The dimensions of photo are 1.2 mm × 1.8 mm. The direction of the loaded diameter of the disk is vertical.

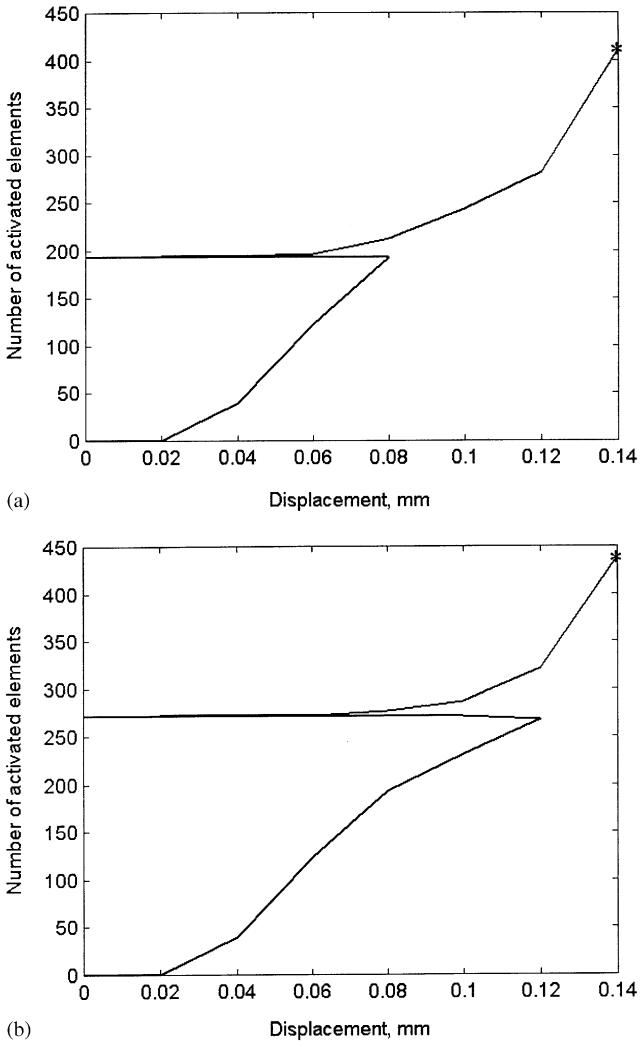

Fig. 12. Number of activated elements vs. displacement for a disk rotation by 4° between first and second cycle and peak displacement of 0.08 mm (a) or 0.12 mm (b) in the first cycle.

in the second cycle, prior to the peak displacement of the first cycle. The trend towards an earlier onset of AE is more pronounced when the peak displacement of the first cycle is 0.12 mm (Fig. 12b). The onset of cracking is observed at about 0.75 and 0.65 of the first-cycle peak displacement in Figs. 12a and b, respectively. The Kaiser inflexion in Figs. 12a and b is well identified, in spite of the increased AE at low loads.

In Fig. 13, the induced fractures at the end of the first cycle (a) and at failure, at the end of the second cycle (b) are shown for the specimen presented in Fig. 12a. The location of the main fracture in Fig. 13 corresponds to the new position of the inserts in the second cycle, as it was observed in the experiments.

By increasing the rotation angle to 8°, a further smoothening of the AE curve is observed (see Figs. 14a and b for the peak displacement of the first cycle of 0.08 and 0.12 mm, respectively). AE in the second cycle starts at about 0.50 and 0.65 of the first-cycle peak displacement in Figs. 14a and b, respectively. In Fig. 15, the induced fractures at failure (at the end of the second cycle) are presented for the specimen, which was loaded to 0.08 mm peak displacement in the first cycle.

The position of the main fracture is clearly affected by the rotation, being aligned approximately along the direction of the loaded diameter in the second cycle. Note however that in all simulated tests, the position of the main fracture does not perfectly coincide with the loaded diameter. This simulation result is in agreement with the experiments.

Complete disappearance of the Kaiser effect occurs when the rotation angle becomes equal to 16°, as observed in the experiments. AE curves obtained from the simulations for the peak values of the first-cycle displacement of 0.08 and 0.12 mm are presented in Figs. 16a and b, respectively. In Fig. 16a, AE in the second cycle starts at 0.02 mm displacement, as for the first cycle, indicating a Felicity ratio equal to 0.25. No inflexion, not even a smooth one, is seen in the second

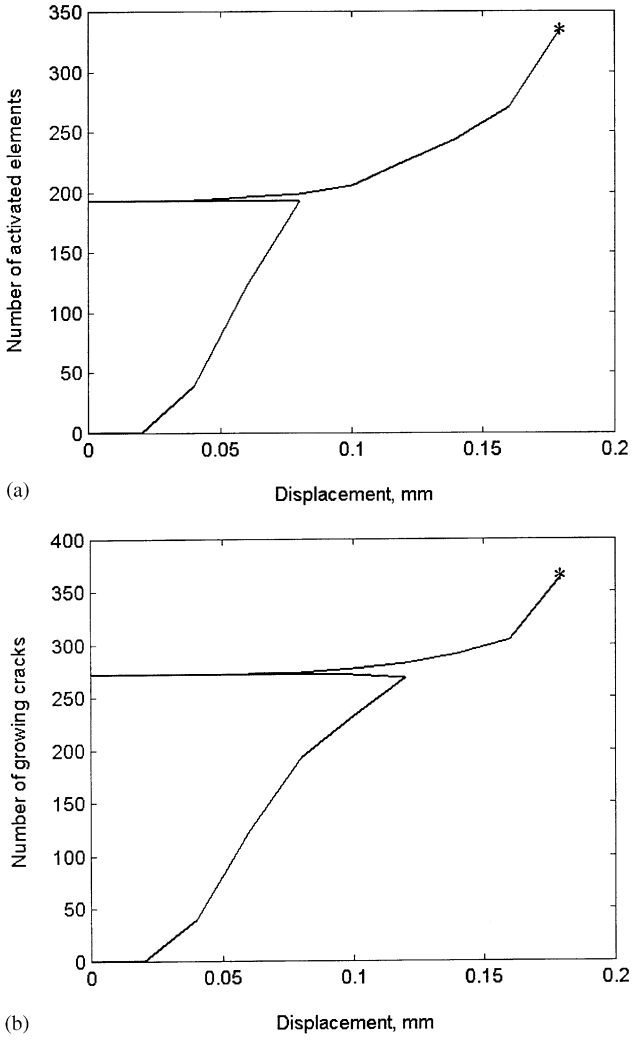

Fig. 14. Number of activated elements vs. displacement for a disk rotation by 8° between first and second cycles and peak displacement of 0.08 mm (a) or 0.12 mm (b) in the first cycle.

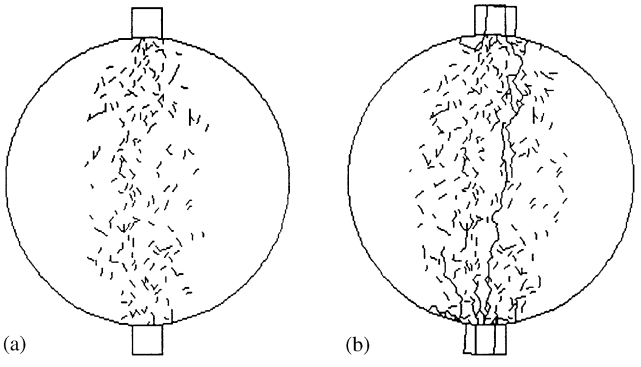

Fig. 13. Induced fractures at the end of the first cycle (a) and at failure, at the end of the second cycle (b) for a disk rotation by 4° between first and second cycles and peak displacement 0.08 mm in the first cycle.

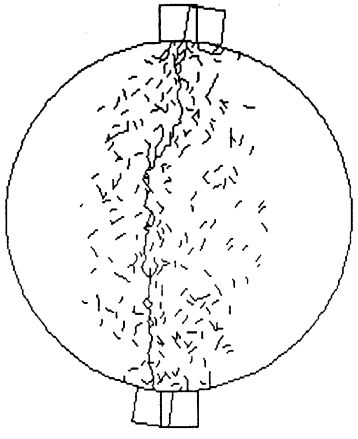

Fig. 15. Induced fractures at failure (at the end of the second cycle) for a disk rotation by 8° between first and second cycles and peak displacement of 0.08 mm in the first cycle.

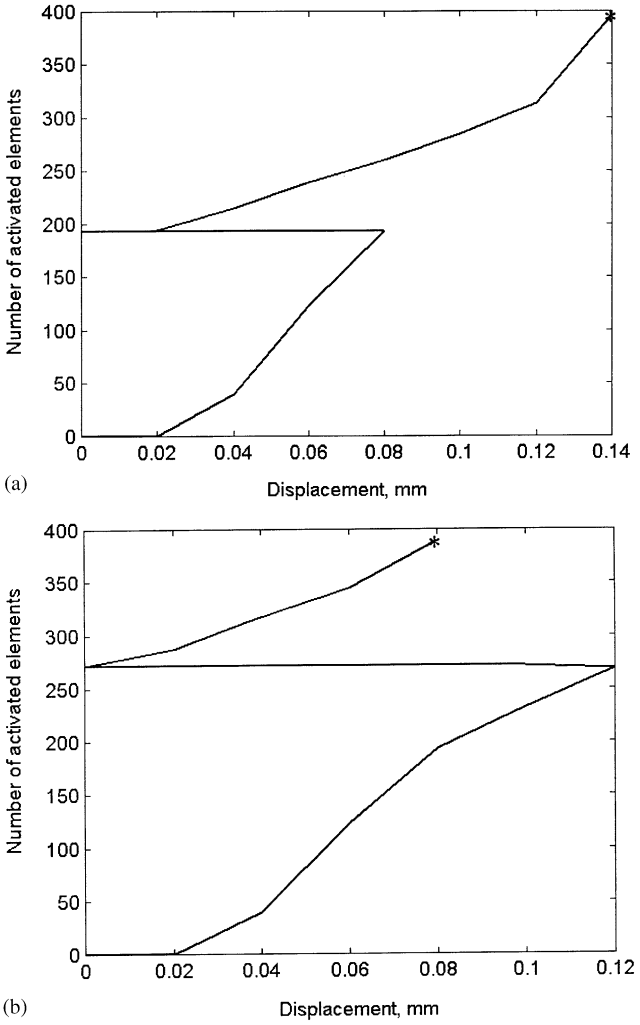

Fig. 16. Number of activated elements vs. displacement for a disk rotation by 16° between first and second cycles and peak displacement of 0.08 mm (a) or 0.12 mm (b) in the first cycle.

cycle at the displacement corresponding to the peak displacement of the first cycle (Fig. 16a). In Fig. 16b, AE takes place from the beginning of loading in the second cycle, probably due to the larger number of elements activated in the first cycle, in comparison to Fig. 16a. The specimen in Fig. 16b fails at a displacement value (0.08 mm) which is lower than the peak displacement of the first cycle (0.12 mm). The point, where the specimen fails, is marked by an asterisk in Fig. 16b. This earlier failure should be attributed to a weakening of the specimen by an anisotropic microcrack population created in the first cycle. The induced fractures corresponding to the 16° test with the peak displacement of the first cycle 0.08 mm (see Fig. 16a) are shown in Fig. 17.

Also for rotation angles of 30°, 46°, 60° and 90° no Kaiser effect was observed. Results for all rotation angles studied are summarized in Figs. 18a and b for the

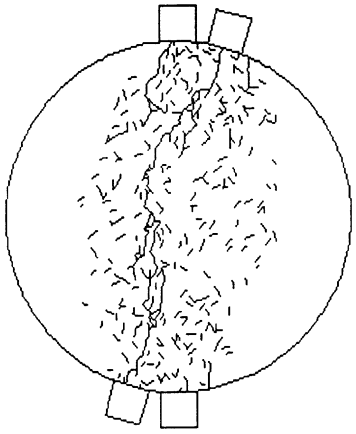

Fig. 17. Induced fractures at failure (at the end of the second cycle) for a disk rotation by 16° between first and second cycles and peak displacement of 0.08 mm in the first cycle.

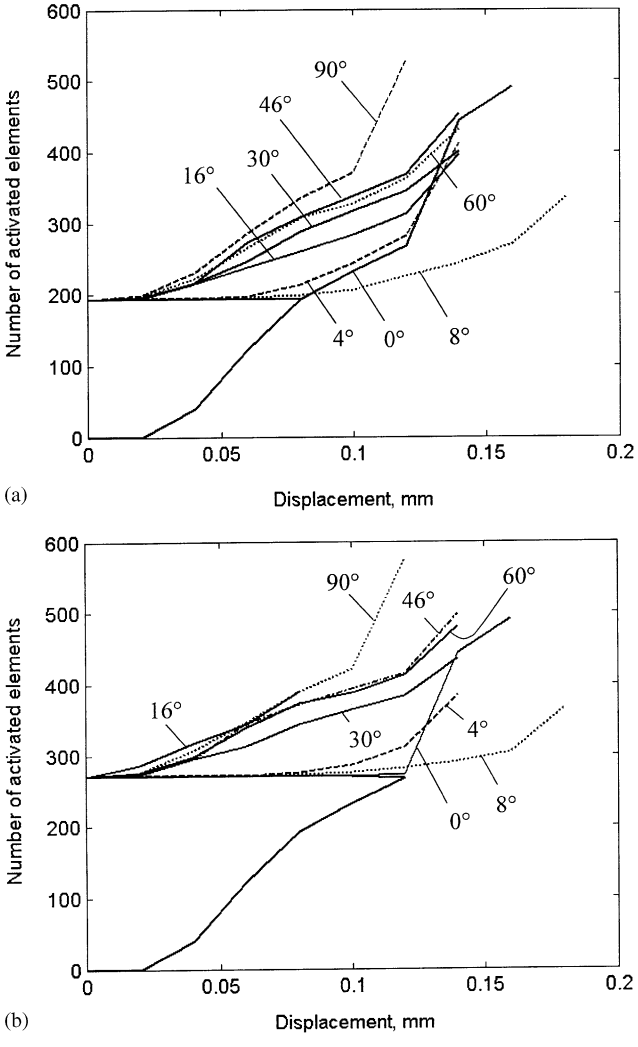

Fig. 18. Number of activated elements vs. displacement in the tests with disk rotation between first and second cycles. Peak displacement 0.08 mm (a) or 0.12 mm (b) in the first cycle.

first-cycle peak displacement of 0.08 and 0.12 mm, respectively. An example of the simulated fractures at failure in the second cycle for the rotation angle of 90° and the peak displacement of the first cycle of 0.08 mm is given in Fig. 19.

It is interesting to look at the microcrack distribution with respect to the type of fracturing (tensile, shear or mixed) and its evolution during loading in the first and second cycle with or without disk rotation. An element is classified as a tensile crack if it is found to fail either by exceeding the tensile strength in both collocation points, or by exceeding the tensile strength at one of the collocation points, while at the other collocation point no failure occurs. An element is classified as a shear crack if it fails either by exceeding the shear strength (according to Coulomb–Mohr envelop) at both collocation points, or by exceeding the shear strength at one of the collocation points, while no failure occurs at the other collocation point. A mixed-type crack is understood to be an element that fails by exceeding the tensile strength in one of the collocation points, while exceeding the shear criterion in the other collocation point.

Data for a test without rotation is summarized in Table 1 (see also Figs. 7b and 8). The peak displacement of the first cycle was 0.08 mm. Hyphens in Table 1 indicate that no new microcracks are formed at the corresponding loading stage. It is clear from Table 1 that at the beginning of loading in the first cycle, almost all cracks belong to the shear type. It corresponds well with the observation that the microcracking starts in the neighborhood of the disk–insert contact in the simulations. The percentage of shear cracks decreases and the percentage of tensile cracks increases gradually during loading in the first cycle. In the second cycle, no new microcracks are observed until the peak displacement of the first cycle is reached. Then, microcracking re-starts. The percentage of the new shear cracks in the second cycle decreases again gradually, beginning from the percentage which was reached at the end of the first cycle. A dramatic increase in the absolute number of tensile cracks is seen only at the moment when the main fracture begins to form (at a displacement of 0.14 mm), leading to a rapid decrease in the percentage of shear cracks and a corresponding dramatic increase in the percentage of tensile cracks. An important conclusion is that the large majority of microcracks at the stages prior to the macrofracturing, are of shear type. This is in full agreement with results of the experimental investigation of AE source types carried out in Ref. [28,39]. The percentage of mixed-type microcracks remains approximately the same during both cycles and is small (1–3%).

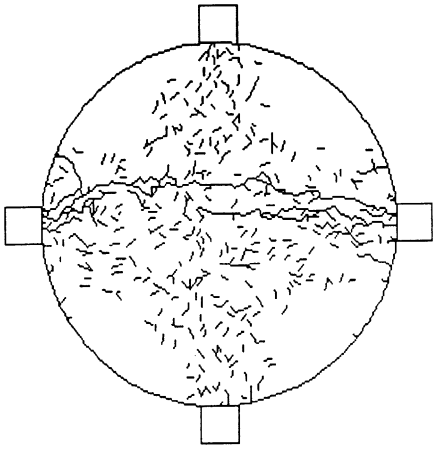

Fig. 19. Induced fractures at failure (at the end of the second cycle) for a disk rotation by 90° between first and second cycles and peak displacement of 0.08 mm in the first cycle.

In the case of a 4° rotation, an earlier reactivation of microcracking in the second cycle was observed. The few microcracks which had formed in the second cycle prior to reaching the peak first-cycle displacement, were all of shear type. The distribution of activated elements with respect to their fracturing type, for a 4°-rotation test is presented in Table 2.

The results of the microcrack distribution analysis for other angles studied (8°, 16°, 30°, 46°, 60° and 90°) were very similar to those for 4°. With increasing rotation angle, microcracks in the second cycle became activated earlier and earlier, and these earlier activated microcracks were predominantly of shear type. The percentage of the shear cracks decreased gradually during the second cycle, and eventually dropped to close to zero when the macrofracture developed.

6. Discussion: experiment vs. simulation

DIGS simulations of the cyclic Brazilian tests without rotation have shown a good agreement with experimental results. Microfracturing is initiated in the vicinity of the loading contacts and is followed by the appearance of microcracks over a wide area around the loaded diameter, resulting finally in a macrofracture. The latter is situated between the two disk–insert contacts, but is mostly slightly curved. Most microcracks are of shear type. The percentage of shear cracks decreases gradually during loading, yet they are dominant until the main fracture is formed. This is in full agreement with the experiments by Falls et al. [28,39], who analysed the type of AE sources using a multi-channel AE system. The macrofracture pattern is close to reality as well, namely disks fail along the loading direction. One or more secondary cracks are observed to run subparallel to the main fracture, and a developed shear zone in the contact area is observed in some cases as well. Simulated microcrack structures correspond well with microscopic observations.

The slope of the envelope curve 'cumulative number of activated elements vs. displacement' in Fig. 7b

Table 1
Distribution of elements with respect to their type in a two-cycle test without rotation ($\theta = 0^\circ$)

Displacement (mm)	Total absolute number of elements activated at the loading step	Shear elements (%)	Tensile elements (%)	Mixed type elements (%)
0	0	—	—	—
0.02	0	—	—	—
0.04	39	97.4 (38[a])	2.6 (1[a])	0 (0[a])
0.06	84	94 (79)	3.6 (3)	2.4 (2)
0.08	70	88.6 (62)	10 (7)	1.4 (1)
0.06	0	—	—	—
0.04	0	—	—	—
0.02	0	—	—	—
0.00	0	—	—	—
0.02	0	—	—	—
0.04	0	—	—	—
0.06	0	—	—	—
0.08	0	—	—	—
0.10	39	87.2 (34)	10.3 (4)	2.5 (1)
0.12	36	80.5 (29)	16.7 (6)	2.8 (1)
0.14	170	7.0 (12)	91.2 (1 5 5)	1.8 (3)
0.16	47	8.5 (4)	89.4 (42)	2.1 (1)

[a] Absolute amount of activated elements of a specific type given between brackets.

Table 2
Distribution of elements with respect to their type in a two-cycle test with rotation ($\theta = 4^\circ$)

Displacement (mm)	Total absolute number of elements activated at the loading step	Shear elements (%)	Tensile elements (%)	Mixed type elements (%)
0	0	—	—	—
0.02	0	—	—	—
0.04	39	97.4 (38[a])	2.6 (1[a])	0 (0[a])
0.06	84	94 (79)	3.6 (3)	2.4 (2)
0.08	70	88.6 (62)	10 (7)	1.4 (1)
0.06	0	—	—	—
0.04	0	—	—	—
0.02	0	—	—	—
0.00	0	—	—	—
0.02	1	100 (1)	0	0
0.04	0	—	—	—
0.06	3	100 (3)	0 (0)	0 (0)
0.08	16	94.0 (15)	6.0 (1)	0.0 (0)
0.10	31	61.3 (19)	38.7 (12)	0.0 (0)
0.12	148	71.0 (27)	26.3 (1 2 0)	2.7 (1)
0.14	130	3.1 (4)	95.4 (1 2 4)	1.5 (2)

[a] Absolute amount of activated elements of a specific type given between brackets.

indicates some fluctuations during the first and second cycles. The slope increases at the points corresponding to the displacement values of 0.02 and 0.04 mm, and decreases at the point with a displacement value of 0.08 mm. This decrease in the slope of the envelope curve at 0.08 mm is due to the inhomogeneity of the specimen as introduced by the random tessellation mesh and random distribution of the weakened elements ('flaws').

The DIGS simulation of the tests with rotation shows good agreement with experimental findings (Table 3). With increase in the rotation angle, the Kaiser effect becomes gradually less pronounced. This is due to an increasing AE level at lower load in the second cycle. Complete disappearance of sample memory is observed for rotation angles larger than 15°, as was theoretically predicted earlier using the Fairhurst–Cook microcracking model [11,16].

Now that a good agreement has been established between the experiments and the simulation results, one can use the numerical approach to study a case where it is not possible to arrange a direct experimental

Table 3
Comparison between experimental and simulation results

Rotation angle (°)	Experimental results	DIGS simulation results
0	Very well-pronounced Kaiser effect with $FR = 0.93-1.00$	Very well-pronounced Kaiser effect with $FR = 1.00$
3.5	Earlier (at low loads) onset of AE in the second cycle. Bilinear interpolation of the cumulative hits vs. load curve allows an unambiguous identification of the Kaiser effect at the peak load of the first cycle	Earlier onset of cracking in the second cycle. Kaiser effect is well identifiable at approximately the peak load of the first cycle
7.5	Further increase of AE activity at low loads. Kaiser effect is observed as a smooth inflexion in the cumulative hits vs. load curve or as an onset of a steadily increasing AE which takes place at the load equal to the first-cycle peak load	Further smoothening of the AE curve
15, 30, 45, 60, 90	Complete disappearance of the Kaiser effect	Complete disappearance of the Kaiser effect

verification. This is due to non-identity of different rock specimens, which makes it not feasible to compare between absolute AE activity values obtained on different samples.

The aim of the simulation below is to compare the number of activated microcracks during loading in a direction in the cases when a previous loading was or was not performed in a perpendicular direction. In Refs. [22–24], it was argued that the crack growth produced by loading in one particular direction is largely unaffected by previous stressing in orthogonal directions. The simulation below allows a deeper insight into the problem. Denote the direction of the preloading (if any) by $D1$, and the direction of the subsequent reloading by $D2$. Directions $D1$ and $D2$ are orthogonal. Three cases are to be analysed:

(1) loading in the direction of $D2$ without pre-loading in the $D1$-direction (i.e. only one loading is performed, and this is in the direction of $D2$);
(2) loading in the direction of $D2$ after a pre-loading in the $D1$-direction up to a displacement of 0.08 mm; and
(3) loading in the direction of $D2$ after a pre-loading in the $D1$-direction up to a displacement of 0.12 mm.

Three simulated curves corresponding to these three cases are shown in Fig. 20. It is clear from Fig. 20 that, although the first cycle (in the direction of $D1$) does not result in a Kaiser effect during the following loading in the direction of $D2$, there is some influence of the first cycle upon the AE activity and crack growth in the second cycle. Namely, the pre-loading in $D1$ direction results in a lower microcracking activity in the second cycle. The microcracking activity in the second cycle will be the lower, the higher the peak displacement reached in the first cycle was (cf. curves 2 and 3 in Fig. 20).

It should be noted again that it was possible to make this conclusion only by using simulations, because in reality it is not possible to test the same specimen several times, and different specimens would give a different

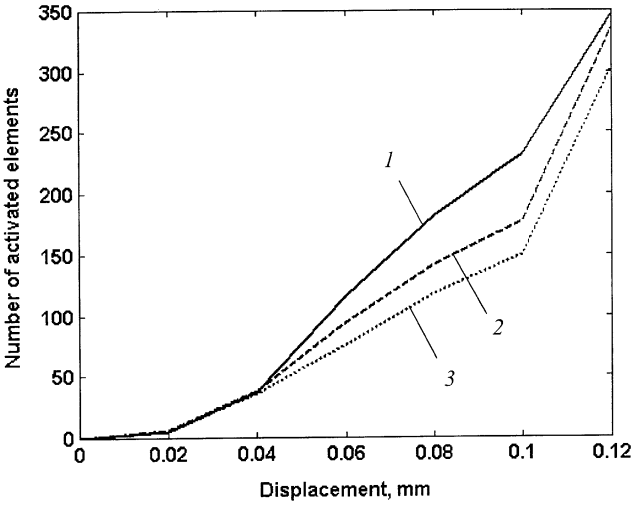

Fig. 20. Number of activated elements vs. displacement during loading of a disk specimen in the direction of $D2$. Curve 1: no pre-loading. Curve 2: after a pre-loading in the direction of $D1$ with a peak displacement of 0.08 mm. Curve 3: after a pre-loading in the direction of $D1$ with a peak displacement of 0.12 mm. Directions $D1$ and $D2$ are perpendicular to each other.

absolute value of AE activity (non-reproducibility of AE in different specimens due to the rock inhomogeneity).

A fundamental difference exists between the Kaiser effect simulation by DIGS code carried out in this paper, and the earlier simulations of the Kaiser effect in Refs. [11,16,20]. In the earlier papers, a three-dimensional model of microcracking under compression was employed, based on the Fairhurst–Cook concept of tensile cracks generated by shear cracks ('wing' crack model). According to this model, during application of load to the rock in the first cycle, tensile microcracks are initiated by shear displacement along initial microcracks and these cracks grow in a stable manner. Their length after completing the first cycle is uniquely defined by the peak stress value reached in the first cycle. As a result, in the second loading cycle, being conducted in the same direction as the first cycle, these cracks re-start growing

only when the applied stress exceeds the peak stress value of the first cycle. The cracks growing in the second cycle are the same as those which were growing in the first cycle.

The formation of the Kaiser effect in DIGS simulations is different from the above-described scheme based on the Fairhurst–Cook model. Cracks in DIGS are represented by discrete elements. These elements, having once been activated, cannot be reactivated for the second time. During the reloading in the second cycle without a rotation, no elements are activated before the peak stress of the first cycle is surpassed because all elements which would be activated, were already activated in the first cycle. After surpassing the peak load of the first cycle, *new* elements become activated, giving rise to AE. These newly activated elements can be connected to already activated elements (thus forming a longer crack) or can be located at a certain distance from them.

In spite of this difference between the two models, their predictions for the angular sensitivity are in good agreement and correspond well with the results of the laboratory tests.

7. Conclusions

Experiments performed on diametrically loaded disk specimens of a brittle rock have demonstrated the high sensitivity of the Kaiser effect to the rotation of the loading directions. The Kaiser effect becomes gradually less pronounced while the rotation angle of principal stress axes between first and second cycle increases from 0° to 7.5°. When the rotation angle reaches 15° the effect disappears completely. This implies that the knowledge of the precise orientation of the in situ σ_1 stress axis is necessary in order to apply the stress memory phenomenon for geo-stress estimations. Inaccuracy in the chosen direction of the test specimen can result in an apparent absence of the Kaiser effect or in some incorrect results. On the other hand, this high directional sensitivity creates a basis for an accurate determination of the direction of the major principal stress.

Acknowledgements

Valuable discussions with Bart Van de Steen, Ewan Sellers and Erik Eberhardt are gratefully appreciated. Thanks are due to Albert Bral, Kris Van de Staey and Johan Vanhulst for their help while preparing the specimens and conducting the tests. The Research Council of the Katholieke Universiteit Leuven is gratefully acknowledged for the financial support of the post-doctoral research fellowship of Alexander Lavrov.

References

[1] Kaiser J. Erkenntnisse und Folgerungen aus der Messung von Geräuschen bei Zugbeanspruchung von metallischen Werkstoffen. Archiv fr das Eisenhttenwesen, 1953;24:43–5.
[2] Li C, Nordlund E. Experimental verification of the Kaiser effect in rocks. Rock Mech Rock Eng 1993;26:333–51.
[3] Barr SP, Hunt DP. Anelastic strain recovery and the Kaiser effect retention span in the Carnmenellis granite, UK. Rock Mech Rock Eng 1999;32:169–93.
[4] Filimonov YL, Lavrov AV, Shafarenko YM, Shkuratnik VL. Memory effects in rock salt under triaxial stress state and their use for stress measurement in a rock mass. Rock Mech Rock Eng 2001;34:275–91.
[5] Hardy Jr HR. Evaluation of in-situ stresses in salt using acoustic emission techniques. In: Proceedings of the Seventh Symposium on Salt, vol. 1. Amsterdam: Elsevier, 1993. p. 49–58.
[6] Lavrov A. Kaiser effect observation in brittle rock cyclically loaded with different loading rates. Mech Mater 2001;33:669–77.
[7] Guyer RA, McCall KR. Hysteresis, discrete memory, and nonlinear wave propagation in rock: a new paradigm. Phys Rev Lett 1995;74:3491–4.
[8] Guyer RA, Johnson PA. Nonlinear mesoscopic elasticity: evidence for a new class of materials. Phys Today 1999; 52(4):30–6.
[9] Johnson PA, Rasolofosaon PNJ. Manifestation of nonlinear elasticity in rock: convincing evidence over large frequency and strain intervals from laboratory studies. Nonlinear Processes Geophys 1996;3:77–88.
[10] Hamstad MA. Discussion of the basic understanding of the Felicity effect in fiber composites. J Acoust Emission, 1986;5(2):95–102.
[11] Holcomb DJ. General theory of the Kaiser effect. Int J Rock Mech Min Sci Geomech Abstr 1993;30:929–35.
[12] Yamshchikov VS, Shkuratnik VL, Lavrov AV. Memory effects in rocks (review). J Min Sci 1994;30:463–73.
[13] Holcomb DJ. Using acoustic emission to determine in-situ stress: problems and promise. In: Proceedings of Applied Mechanics, Bioengineering and Fluids Engineering Conference, Houston, 1983. p. 11–21.
[14] Pestman BJ, Van Munster JG. An acoustic emission study of damage development and stress-memory effects in sandstone. Int J Rock Mech Min Sci Geomech Abstr 1996;33:585–93.
[15] Filimonov YL, Lavrov AV, Shkuratnik VL. Prospects of memory effects for stress measurement applications in rock salt. In: Proceedings of the EUROCK'2001 Symposium. Rotterdam: A.A.Balkema, 2001. p. 59–63.
[16] Lavrov AV. Three-dimensional simulation of memory effects in rock samples. In: Sugawara K; Obara Y, editor. Rock stress. Proceedings of the International Symposium on Rock Stress. Rotterdam: A.A.Balkema, 1997. p. 197–202.
[17] Li C. A theory for the Kaiser effect and its potential applications. In: Proceedings of the Sixth Conference on AE/MA in Geologic Structures and Materials. Clausthal-Zellerfeld: Trans Tech Publications, 1998. p. 171–85.
[18] Shkuratnik VL, Lavrov AV. Numerical simulation of the Kaiser effect under triaxial stress state. Proceedings of the Third International Conference on Mechanics of Jointed and Faulted Rock (MJFR-3). Rotterdam: A.A.Balkema, 1998. p. 381–5.
[19] Lavrov AV, Yasinski MV. On the influence of intermediate principal stress upon acoustic emission in cyclically loaded rocks. In: Proceedings of the Tenth Session of the Russian Acoustical Society. Moscow: GEOS, 2000. p. 211–4 [in Russian; extended abstract in English at URL: http://www.akin.ru/e_main.htm].

[20] Lavrov A. Theoretical investigation of the Kaiser effect manifestation in rocks after true triaxial pre-loading. Arch Min Sci 2001;46:47–65.
[21] Holt RM, Pestman BJ, Kenter CJ. Use of discrete particle model to assess feasibility of core based stress determination. In: Proceedings of the DC Rocks 2001, US Symposium on Rock Mechanics, July 7–10. Washington, DC, Rotterdam: A.A.Balkema, 2001.
[22] Stuart CE, Meredith PG, Murrell SAF, Van Munster JG. Anisotropic crack damage and stress-memory effects in rocks under triaxial loading. Int J Rock Mech Min Sci Geomech Abstr 1993;30:937–41.
[23] Michihiro K, Hata K, Yoshioka H, Fujiwara T. Determination of the initial stresses on rock mass using acoustic emission method. J Acoust Emission 1991/1992;10(1/2):S63–76.
[24] Stuart CE, Meredith PG, Murrell SAF. Acoustic emission study of anisotropic stress memory in rock subjected to cyclic polyaxial loading. J Acoustic Emission 1994;12(3/4):S12–7.
[25] Napier JAL, Hildyard MW. Simulation of fracture growth around openings in highly stressed, brittle rock. J S Afr Inst Min Metall 1992;92(6):159–68.
[26] Napier JAL. Modelling of fracturing near deep level gold mine excavations using a displacement discontinuity approach. In: Rossmanith HP, editor. Mechanics of jointed and faulted rock. Rotterdam: A.A.Balkema, 1990. p. 709–15.
[27] Brown ET. Rock characterization testing and monitoring ISRM suggested methods. Oxford: Pergamon Press, 1981.
[28] Falls SD, Chow T, Young RP, Hutchins DA. Acoustic emission analysis and ultrasonic velocity imaging in the study of rock failure. In: Sachse W, Roget J, Yamaguchi K, editors. Acoustic emission: current practice and future directions, ASTM STP 1077. Philadelphia: American Society for Testing and Materials, 1991. p. 381–91.
[29] Van de Steen B, Wevers M. Acoustic emission preceding macro crack formation in samples containing a stress concentrator. In: Rossmanith HP, editor. Proceedings of the International Conference on Mechanics of Jointed and Faulted Rock (MJFR-3). Rotterdam: A.A.Balkema, 1998. p. 387–92.
[30] Crouch SL, Starfield AM. Boundary element methods in solid mechanics. London: George Allen & Unwin, 1983.
[31] Van de Steen B, Vervoort A, Napier JAL. Numerical simulation of fracture initiation and propagation in biaxial tests on rock samples. Int J Fract 2001;108:165–91.
[32] Van de Steen B, Vervoort A, Jermei J. Crack initiation at a heterogeneity in a rock sample subjected to the Brazilian test. In: Rossmanith HP, editor. Proceedings of the International Conference on Mechanics of Jointed and Faulted Rock (MJFR-3). Rotterdam: A.A.Balkema, 1998. p. 357–62.
[33] Van de Steen B. Effect of heterogeneities and defects on the fracture pattern in brittle rock. Ph.D. thesis. Catholic University of Leuven, 2001, 250pp.
[34] Colback PSB. An analysis of brittle fracture initiation and propagation in the Brazilian test. In: Proceedings of the First Congress of the International Society of Rock Mechanics, Lisbon, 1966. p. 385–91.
[35] Tang CA, Kaiser PK. Numerical simulation of cumulative damage and seismic energy release during brittle rock failure—Part I: fundamentals. Int J Rock Mech Min Sci Geomech Abstr 1998;35:499–518.
[36] Holt RM, Brandshaug T, Cundall PA. Discrete particle and laboratory modelling of core mechanics. In: Proceedings of the Fourth North American Rock Mechanics Symposium. Narms 2000, July 31–August 3, Seattle, Washington, USA. Rotterdam: A.A.Balkema, 2000.
[37] Napier JAL, Malan DF. A viscoplastic discontinuum model of time-dependent fracture and seismicity effects in brittle rock. Int J Rock Mech Min Sci 1997;34:1075–89.
[38] Hazzard JF, Young RP. Simulating acoustic emissions in bonded-particle models of rock. Int J Rock Mech Min Sci Geomech Abstr 2000;37:867–72.
[39] Falls SD, Chow T, Young RP, Hutchins DA. Acoustic emission analysis and ultrasonic velocity imaging in the study of rock failure. J Acoust Emission 1989;9(1/2):S166–9.
[40] Lavrov AV. Acoustic emission during Brazilian tests of a brittle rock. In: Proceedings of the 11th Session of the Russian Acoustical Society, vol. 2. Moscow: GEOS, 2001. p. 99–102 [in Russian].
[41] Lavrov AV, Vervoort A, Napier JAL. Damage development in rock subjected to cyclic loading. In: Proceedings of the Second Biot Conference on Poromechanics. Rotterdam: A.A.Balkema, 2002, in print.